Published in final edited form as:
J Orthop Res. 2013 April ; 31(4): 621–631. doi:10.1002/jor.22281.

Structural, Compositional, and Biomechanical Alterations of the Lumbar Spine in Rats with Mucopolysaccharidosis Type VI (Maroteaux–Lamy Syndrome)

Alon Lai[1], **Calogera M. Simonaro**[2], **Edward H. Schuchman**[2], **Yi Ge**[2], **Damien M. Laudier**[1], and **James C. Iatridis**[1]

[1]Leni and Peter W. May Department of Orthopaedics, Mount Sinai School of Medicine, New York, New York

[2]Department of Genetics and Genomic Sciences, Mount Sinai School of Medicine, New York, New York

Abstract

Mucopolysaccharidosis (MPS) VI is an inherited lysosomal storage disorder resulting from deficiency of *N*-acetylgalactosamine-4-sulfatase activity and subsequent accumulation of incompletely degraded dermatan sulfate (DS) containing glycosaminoglycans (GAGs). Painful spinal deformities are commonly found in MPS VI patients. We characterized lumbar spine structure, composition, and biomechanics in a naturally occurring rat MPS VI model and evaluated the role of MMP-13, ADAMTS-5 and TNF-α in modulating the observed changes. MPS VI rats had discs with large vacuolated cells and sizable nuclear defects. MPS spine segments also had structural and functional changes suggestive of spinal instability, including decreased nuclear pressurization, increased joint laxity and increased disc height index. These functional changes were at least partly associated with elevated ADAMTS-5, MMP-13, and TNF-α. Vertebral and endplate biomechanics were also affected by MPS VI with decreased failure load and stiffness. The discal and vertebral dysfunctions observed in MPS VI rats are likely to be associated with pathological spinal conditions, similar to those that afflict MPS patients. Our findings also suggest more broadly that abnormal accumulation of GAGs and the associated chronic pro-inflammatory and catabolic cascade may also be a source of spinal dysfunction.

Keywords

mucopolysaccharidosis VI; biomechanical properties; TNF-α; MMP-13; ADAMTS-5

Mucopolysaccharidosis VI (MPS VI or Maroteaux–Lamy syndrome) is a rare, inherited lysosomal storage disorder due to mutations in the gene encoding *N*-ace-tylgalactosamine-4-sulfatase, (NG4S, arylsulfatase B), located on chromosome 5.[1] NG4S is responsible for catalyzing the hydrolysis of 4-sulfate groups in glycosaminoglycans (GAGs), particularly dermatan sulfate (DS).[2] The deficiency of NG4S activity results in incomplete degradation and cellular accumulation of DS.[3] Clinically, MPS VI is associated with short stature, skeletal abnormalities, dysostosis multiplex, cranial and tracheal abnormalities, hearing loss, cornea and cardiovascular defects, and degenerative joint disease.[3] In the spine, patients commonly have abnormally developed vertebral bodies that are associated with a high incidence of spinal deformity (e.g., scoliosis and kyphosis), spinal instability, and stenosis

Correspondence to: James C. Iatridis (T: 212-241-1517; F: 212-876-3168, james.iatridis@mssm.edu).

that are a common source of back pain.[3,4] Spinal cord compression might be associated with severe spinal instability and spinal stenosis, and surgical interventions might be required for decompression and stabilizing the spine to prevent paralysis.[3,4] While no systematic study exists on back pain in MPS patients, an informal verbal poll by the authors found 7 of 10 MPS VI patients suffered from low back pain.[5] However, etiology of MPS VI related spinal dysfunction and their associated changes in structure and biomechanics of intervertebral discs (IVD) and vertebrae are not well known.

The lumbar spine of canines with MPS VII (or Sly syndrome) was recently investigated by Smith et al.[6] who found many structural, biochemical, and biomechanical alterations. MPS VII is associated with a deficiency in β-glucuronidase activity leading to systemic accumulation of incompletely degraded chondroitin, dermatan and heparin sulfate, and shared orthopaedic characteristics with MPS VI, including joint contractures and dysostosis multiplex.[4] It is important to determine if this compelling data for MPS VII in canines is similar in other species with other MPS disorders.

Naturally occurring animal models of MPS VI were described in rats and cats, and exhibit similar phenotypic characteristics as human MPS VI patients.[2,7–10] MPS VI rats exhibited articular cartilage with increased apoptotic chondrocytes, depletion of total proteoglycan and collagen, and up-regulation of tumor necrosis factor alpha (TNF-α), nitric oxide, and matrix metalloproteinase (MMP)-2 and -9.[11,12] Systemic disorders affecting hyaline cartilage often impact intervertebral discs because of the similarities in composition and limited vascularity and nutrient transport. Spinal instability and stenosis are common in MPS disorders,[4] suggesting that functional spinal biomechanics are likely to be altered with disease. Consequently, improved characterization of spine pathologies associated with MPS VI disorders are a priority.

We investigated the structural, compositional, and biomechanical alterations of lumbar spines in a naturally occurring MPS VI rat model. Our findings provide insight into the development and progression of spinal pathologies in MPS disorders, may suggest ways to intervene, and also inform how accumulation of incompletely degraded intracellular DS affects the spinal system. We hypothesized that MPS VI results in spinal deformity and functional biomechanical alterations that can lead to instability, and that abnormal accumulation of DS further predisposes to spine dysfunction via increased catabolism modulated by the up-regulation of TNF-α.

METHODS

Healthy normal ($n = 6$) and MPS VI ($n = 6$) Sprague–Dawley rats were used (Fig. 1); the MPS VI rat model was previously characterized.[2,12–14] All rats were raised at the Mount Sinai School of Medicine following NIH and USDA guidelines regarding animal care and use. Rats were euthanized at 6–7 months old using carbon dioxide inhalation. Lumbar spines were isolated, and the soft tissues and zygapophyseal joints were removed. Motion segments for histology and immunohistochemistry were fixed in buffered 10% formalin; those for biomechanical, radiological, and biochemical analyses were frozen until testing.

L1–L2 motion segments were used for histology and were embedded in methyl methacrylate and sectioned at 5 μm. Mid-sagittal sections were stained with Safranin-O/fast-green/hematoxylin. L4–L5 IVDs were used to determine IVD water and GAG contents. Motion segments were frozen using liquid nitrogen during processing to minimize loss of water or gelatinous nucleus pulposus (NP). Frozen IVDs were separated into NP and annulus fibrosus (AF) using 1.5 mm biopsy punches (Acuderm, Inc., Fort Lauderdale, FL). NP and AF wet tissue weights were measured, and then lyophilized (−40°C for 24 h) to obtain dry tissue

weight. Percent water content was calculated as (wet tissue weight–dry tissue weight)/wet tissue weight × 100%. Lyophilized tissue was then digested using papain extracting reagent (Fisher Scientific, Pittsburgh, PA) overnight at 65°C. Sulfated GAG content was measured using Blyscan assay, normalized by the dry tissue weight.[15]

The disc height index (DHI) of the L5–L6 disc was measured using lateral radiographs with a step wedge as a reference for grayscale intensity and linear dimensions.[16] Intervertebral distances were measured and normalized to adjacent vertebral lengths to obtain the DHI (Fig. 2). L5–L6 motion segments were then prepared for biomechanical assessment by potting in two 10 mm diameter stainless steel tubes using cyanoacrylate and a custom clamp to insure alignment.

Motion segment biomechanical properties were assessed via axial tension–compression and torsional experiments. Axial biomechanics were evaluated using an Enduratec ELF 3200 testing machine (Bose Corporation, Eden Prairie, MN) with a force-controlled testing protocol.[17] Potted specimens were tested in a fluid bath of PBS solution with protease inhibitor (complete cocktail tablet, Roche Diagnostics Corporation, Indianapolis, IN). The testing protocol consisted of three loading stages: (A) equilibration (−1.875 N for 30 min) as a baseline for both axial and torsional tests,[17] (B) cyclic tension-compression test (±6.25 N for 20 cycles at 1 Hz), and (C) creep test (−6.25 N for 60 min). For cyclic and creep tests, the maximum compressive load of 6.25 N was chosen to apply a compressive stress equivalent to ~0.5 MPa, which corresponds to intradiscal pressure in humans during relaxed standing.[18] Torsional biomechanical properties were assessed using an AR 2000ex rheometer (TA Instruments, New Castle, DE). The specimens were tested using a rotation-controlled approach with two loading stages: (1) equilibration (−6.25 N for 30 min) and (2) cyclic rotation test (±10°in both directions at 1 Hz). Ten degree of rotation was chosen to insure both neutral zone (NZ) and linear region characteristics were included.[19,20]

For axial cyclic and torsional testing, data from the last cycle was used for analysis.[17,20–22] Both NZ and linear region characteristics were determined. The NZ region was identified using the mathematical approach of Smit et al.,[23] and the NZ length and stiffness were determined. For the axial linear region characteristics, a line was fit through the data points between 70% and 100% of the minimum and maximum load to determine the compressive and tension stiffness, respectively. For the torsional test, the linear stiffness was defined as the average of the slopes of the lines fitting between 50% and 100% of the minimum and maximum torque. The torque range was defined as the total range of torque applied over the 10°angular displacement in both directions.[19,20] For the creep test, the time-dependent displacement was fit to a stretched exponential function to obtain creep displacement and time constant.[17,21] Geometric differences between normal and MPS IVDs were taken into account in calculating the IVD biomechanical behaviors. For the axial cyclic test, the NZ compressive and tension stiffnesses (S, N/mm) were normalized to the disc height (h, mm) and area (A, mm^2) using $E_{APP} = Sh/A$, where E_{APP} is the apparent modules for NZ compression and tension regions.[22,24] Creep displacement was normalized by dividing by IVD height.[24] Torsional stiffness (K, Nmm/°) of NZ and linear regions were normalized to disc height (h, mm) and polar moment of inertia (J, mm^4) using $G_{APP} = Kh/J$, where G_{APP} is the apparent shear modulus for NZ and linear regions.[19,21,22] All analyses procedures were performed using Matlab Software (R2011a, MathWorks, Inc., Natick, MA).

Vertebral endplate biomechanics were assessed on L6 vertebrae that were isolated by cutting through the L5–L6 disc following motion segment testing. The specimen was attached to a uniaxial testing machine (Instron 8872, Instron, Norwood, MA) with custom grips. A 0.8 mm diameter spherical tip was indented into the center of the bone at the rate of 0.2 mm/s to a depth of 2 mm.[625] The specimens were tested in PBS solution with protease inhibitor.

Only the central region was tested due to the limitation of vertebral size. The single point measurement of endplate stiffness was also justified by Smith et al.[6] who showed no regional differences in endplate biomechanics of MPS VII and normal canine vertebrae. Endplate stiffness and failure load were determined from load-displacement curves with stiffness being the linear region slope and failure load being the maximum load preceding a rapid force decrease.[25,26]

Vertebral bone biomechanics were quantified using fracture testing on L3 or L4 vertebrae using the Instron machine with flat compression platens in PBS solution with protease inhibitors. Posterior elements and surrounding soft tissues were removed, and superior and posterior endplates were minimally shaved flat to insure the vertebral body could align vertically and perpendicularly to the loading axis.[26] The upper platen compressed the specimen at 0.05 mm/s to a depth of 2 mm, and the vertebral stiffness and failure load were determined.[25,26]

Mid-sagittal sections of L1–L2 motion segments were used for immunohistochemical assessment of ADAMTS-5, MMP-13, and TNF-α. After incubation with hydrogen peroxide to block endogenous peroxidase activity, the sections were treated with antigen retrieval solution (DeCal retrieval solution HK089-5K, Biogenex, Fremont, CA), and non-specific binding sites were blocked using protein block (X0909, Dako, Carpinteria, CA). The sections were then incubated overnight at 4°C with rabbit polyclonal primary antibodies against rat ADAMTS-5 (1:100 dilution, ab41037, Abcam Plc, Cambridge, MA), MMP-13 (1:25 dilution, ab75606, Abcam Plc), and TNF-α (1:500 dillution, ab66579, Abcam Plc). After several rinses with distilled water, sections were incubated with horseradish peroxidase-conjugated secondary antibody, and followed by diaminobenzidine-based peroxidase substrate (ImmPACT DAB, Vector Labs, Burlingame, CA). Sections were counter-stained with methylene blue, dehydrated, mounted, and evaluated using bright-field light microscope with a linear polarizer for presence and distribution of immunostaining. The positively stained cells in NP and AF were located, and the percentage of immunopositive cells was determined and compared between groups. For the negative controls, titered, non-immune normal rabbit serum (Rabbit IgG Serum, Biocare Medical, Concord, CA) was used instead of the primary antibody to confirm that no “false-positive” staining had occurred. Blocks of rat cartilage known to be immunopositive for MMP13 were used as positive control to further validate the staining protocol and antibody specificity.

The differences in DHI, disc compositions, motion segment biomechanics, and vertebral biomechanics between normal and MPS VI samples were compared using unpaired Student’s *t*-test. The percentage of immunopositive cells in MPS disc was compared with normal control using Mann–Whitney test. All statistical tests were performed using SPSS v. 18 Software (SPSS, Inc., Chicago, IL) with level of significance set at $p < 0.05$.

RESULTS

There were marked differences in the structure of the MPS VI disc compared to normal disc (Fig. 3). The annular lamellae were well organized and surrounded the NP with a clear nuclear/annular boundary. The height of the MPS disc was slightly larger than that of normal discs, indicating no signs of “age-related disc degeneration” in the MPS VI animals. However, MPS discs contained sizable NP defects and irregularities in vertebral endplate morphology with less Safranin-O staining than healthy controls. NP and AF cells of MPS VI rats were large and vacuolated, and also had less Safranin-O staining than for controls.

The averaged nuclear and annular GAG contents were similar between MPS and normal discs (normal NP: 113.6 ± 31.3 μg GAG/mg dry weight; normal AF: 55.4 ± 14.2 μg GAG/

mg dry weight; MPS NP: 115.9 ± 56.8 μg GAG/mg dry weight; MPS AF: 54.5 ± 28.5 μg GAG/mg dry weight; $p > 0.05$). There was a trend towards higher water content in both NP and AF of MPS spines than normal spines (normal NP: 69.7 ± 6.0%; normal AF: 60.8 ± 4.5%; MPS NP: 73.7 ± 11.8%; MPS AF: 64.4 ± 2.4%), but the differences were not significant ($p > 0.05$).

The DHI of MPS spines were significantly larger than that for normal ($p < 0.05$), mainly due to the significantly shortened MPS vertebra ($p < 0.05$, Fig. 2). The average disc height of MPS motion segments was slightly larger than that of controls, but the difference was not significant ($p = 0.18$). A qualitative decreased bone density in MPS vertebrae was found compared to normal spines (Fig. 2).

Motion segment biomechanics were significantly affected by MPS VI (Fig. 4). In the axial cyclic test, the MPS motion segments had significantly larger NZ length and smaller NZ stiffness (248% and 27% of normal, respectively, $p < 0.05$). The creep time constant of MPS spines was significantly smaller than that of normal spines (55% of normal, $p < 0.05$). The overall displacement loss (including equilibration, cyclic test, and creep test) was significantly greater for MPS spines (128% of normal, $p < 0.05$). Similar to the axial cyclic test, torsional testing showed significantly larger NZ length and smaller NZ stiffness in the MPS motion segment (131% and 26% of normal, respectively, $p < 0.05$; Fig. 5). The linear stiffness and torque range were also significantly lower for MPS spines (35% and 17% of normal, respectively, $p < 0.05$).

Both vertebral and vertebral endplate biomechanics were markedly affected by MPS (Fig. 6). The stiffness and failure load of MPS VI rat lumbar vertebra were significantly smaller than those of normal vertebra ($p < 0.05$). The vertebral endplate stiffness and failure load in MPS spine were smaller; however, differences were not significant ($p > 0.05$).

ADAMTS-5, MMP-13, and TNF-α-expressing cells were elevated in both NP and AF of the MPS disc compared to normal (Figs. 7–9). The percentages of immunopositive cells in MPS discs for ADAMTS-5 (54% vs. 15%), MMP-13 (53% vs. 13%), and TNF-α (29% vs. 7%) were significantly higher than those in normal controls ($p < 0.05$).

DISCUSSION

We examined the structural, compositional, and biomechanical alterations in lumbar spine using the naturally occurring MPS VI rat model. MPS VI rats share many similar phenotypes to MPS patients, particularly shortened body length and abnormal skulls and dentition.[3] MPS VI rats also exhibited abnormal vertebral development with shorter vertebral length and lower bone density, and had many functional biomechanical alterations including diminished vertebra and vertebral endplate stiffness and failure load, increased axial NZ length and overall displacement, and increased torsional NZ length and reduced torsional stiffness. These conditions could all contribute to scoliotic and kyphotic deformity, spinal instability, vertebral fracture, and back pain associated with MPS patients. The accumulation of DS in MPS VI rats induces TNF-α mediated inflammation with increased MMP-13 and ADAMTS-5 production. Consequently, the functional changes observed in the lumbar spines of MPS VI rats are likely associated with diminished disc and vertebra tissue quality due to increased inflammation in addition to deformity and structural alterations that occurred during development.

Motion segment function and stability are associated with the structure and composition of NP, AF, and vertebrae. The torsional tests loaded AF collagen fibers with little NP pressurization, thereby characterizing AF structure. The reduced torsional stiffness and increased NZ length and torque range of MPS rats reflected diminished AF structure and

collagen integrity. Spinal instability and back pain are associated with alterations in motion segment biomechanics including NZ changes.[27] The decreased NZ stiffness with increased NZ length and torque range revealed that the MPS spine is predisposed to larger motions under small loads. This increased potential for instability can be attributed to material property differences because annular collagen is degraded from increased MMP-13, or structural differences since the intervertebral space is increased. Increased joint thickness was also observed in MPS VI articular cartilage,[28] which can result from abnormalities in matrix formation, increased GAG accumulation, or collagen degradation due to accumulation of pro-inflammatory cytokines and increased enzymatic degradation.

Axial testing examined characteristics of both NP and AF. During axial loading, the central gelatinous NP is compressed, and the pressurized NP is restrained by the circumferential tension in the collagenous AF. The decreased axial NZ stiffness, creep time constant, and increased overall displacement loss in MPS spines are likely due to decreased nuclear pressurization. The decreased pressurization may be associated with the degradation of aggrecan resulting from up-regulation of ADAMTS-5. Aggrecan is the major proteoglycan in the IVD that functions to hold water;[29] the water retention ability of degraded aggrecan was likely diminished resulting in increased water loss and reduced discal pressurization. The AF generates circumferential hoop stresses to stabilize the spine under compressive loadings. The diminished annular stiffness resulting from degradation of annular collagen may also contribute to the altered axial biomechanics observed in MPS VI.

The increased ADAMTS-5 and MMP-13 production are likely regulated by increases in TNF-α and other pro-inflammatory cytokines, which are commonly found in degenerated and herniated discs.[30,31] Seguin et al.[32] investigated the production of matrix and matrix degrading enzymes in NP tissues in response to incubation with TNF-α and found TNF-α decreased aggrecan and collagen II gene expression, reduced the accumulation and synthesis of aggrecan and collagen, and increased expression of MMP-1, MMP-3, MMP-13, ADAMTS-4, and ADAMTS-5. TNF-α was also demonstrated to decrease viability and proliferation of bovine chondrocytes, promote apoptosis, and increase nitric oxide production.[33]

TNF-α can also up-regulate substance P, a neuropeptide associated with pain transmission,[34] and increase the expression of nerve growth factor,[35] which might also facilitate penetration of peripheral nerve growing into the disc and induce back pain.[36,37] Consequently, back pain symptoms observed in MPS VI patients may be associated with a chronic inflammatory state as well as mechanical back pain associated with spinal instability.

The increased catabolism and TNF-α observed in the spines of MPS rats were a systemic response, since increased TNF-α and nitric oxide and marked depletion of proteoglycan and collagen were observed in MPS VI articular cartilage.[12] The increase in TNF-α is likely associated with abnormal matrix composition and abnormal mechanical stress.[12] The DS accumulated in the MPS VI cells is a complex polysaccharide and stimulates nitric oxide release by chondrocytes,[12] which is the primary inducer of chondrocyte apoptosis.[38,39] The increase in cell death can result in abnormal matrix composition with decreased GAG content and reduced production of proteoglycans and collagens.[12] IVD biomechanics and function are also altered with MPS VI, which can lead to abnormal discal stress, increased microfailure, and up-regulation of TNF-α.[40,41] TNF-α might further increase matrix degradation by enhancing the production of matrix degradation enzymes. The chronic pro-inflammatory state in MPS VI rats was measured in these mature animals but may also be present early and impact developmental stages. We infer that accumulation of DS in MPS VI rats are responsible for the pro-inflammatory cascade observed. However, our Blyscan

measurements did not detect differences in GAG content that may be associated with measurable changes being below the resolution of our measurements or due to increased loss of GAG resulting from structural defects and collagen network degradation. The precise pathomechanisms of MPS VI and duration of this pro-inflammatory state in the spine warrants further investigation, and might be different from that of chondrocytes due to differences in cartilage structure, morphology, and cell lineages. Together, our results suggest that anti-inflammatory cytokine treatments could be a target to help control the development or progression of spinal dysfunction in MPS VI patients.

Vertebrae and vertebral endplate biomechanics were also affected by MPS VI with decreases in stiffness and failure load, which might be associated with abnormal development of vertebral bone. Radiographic analysis showed that the MPS vertebral bone was abnormally developed with shorter vertebral length and lower bone density. Barak et al.[42] found that removal of up to 42% of the trabecular bone did not significantly affect the vertebral stiffness, but the vertebral strength was significantly reduced when even smaller amount of trabecular tissue was removed. Tommasini et al.[26,43] found that the vertebral biomechanics were associated with the amount, distribution and quality of both cortical and trabecular bone tissues. Therefore, the structure of the MPS vertebral bones should be studied further to explore the potential mechanism for the changes of biomechanical properties in both vertebra and vertebral endplate.

Lumbar spines of dogs with MPS VII exhibited vertebral endplates that were biomechanically weakened with lower stiffness and failure load.[6] MPS VII motion segments also had higher range of motion and lower stiffness in axial tension–compression suggesting a predisposition for instability, leading Smith et al. to suggest that biomechanical alterations might be associated with spinal deformity observed in MPS VII patients. Moreover, they also demonstrated that the MPS VII discs had elevated GAG with higher water content in AF and epiphyses and lower calcium in the epiphyses, which are associated with the observed biomechanical alterations. The findings on the canine MPS VII model are similar and complementary to findings observed in our rat MPS VI model, suggesting that MPS disorders have many similarities in their musculoskeletal manifestations across species and across the specific types of MPS disorders.

The spinal muscles, ligaments, and posterior elements were removed to facilitate the measurement of motion segment biomechanics, yet in living spinal systems all these structures can play important roles in the spinal motion, stability, and back pain.[27] Removal of these structures also reduces applied axial stresses on the motion segment and can impact IVD height measurements. This dissection was necessary for biomechanical testing, but may have increased variance in disc height measurements preventing us from interpreting the slight increase in disc height in MPS animals as a trend. In our study, the DHI was increased with MPS VI, but was mostly strongly influenced by the reduced vertebral length in MPS animals and amplified potential differences in the disc height between animals. DHI is commonly used as a relative measurement of disc height across species to account for differences in animal size. A loss of DHI is a sensitive measurement of early degenerative changes in the IVD without any changes in vertebral length.[16] In this context, DHI increase (in MPS) and decrease (in degeneration models) both represent sensitive measures of structural alterations and spinal dysfunction.

The decreased bone density in MPS vertebrae was a qualitative observation using plain radiographs, which remains relatively insensitive when compared to quantitative micro-CT and dual-energy X-ray absorptiometry analyses. Micro-CT analyses are recommended for future investigations of bone mineral density and morphology. ADAMTS-5, MMP-13, and TNF-α were chosen for immunohistochemical analyses since they are well accepted

markers of catabolism and inflammation. Additional enzymes and pro-inflammatory cytokines are likely also affected by MPS VI and contribute to changes in spinal biomechanics.

In conclusion, structural, compositional, and functional biomechanical alterations were found in lumbar spines of MPS VI rats that are known to be associated with mechanical back pain (i.e., spinal instability, deformity, vertebral fracture). These changes were associated with deformity and diminished tissue quality that could occur through improper or incomplete development and inferior remodeling. Spinal degeneration may further progress in MPS VI through chronic inflammation and increased matrix catabolism in the spine, that we infer to be associated with excess accumulation of DS and a systemic pro-inflammatory response through the activation of the Toll-like receptor 4 (TLR4) signaling pathway.[13] The altered spinal biomechanics (decrease in nuclear pressurization and increase joint laxity) are likely associated with increased ADAMTS and MMP-13 production, which might be regulated by TNF-α. Therefore, our results suggest that in addition to enzyme replacement therapy and gene therapy, anti-inflammatory treatment directed against TNF-α might offer potential to control the development or progression of pathological spinal conditions in MPS VI patients.

Acknowledgments

Grant sponsor: National Institute of Arthritis and Musculoskeletal and Skin Diseases/National Institutes of Health; Grant numbers: 5R01 AR051146; 1R01 DK087185; Grant sponsor: National MPS Society.

References

1. Litjens T, Baker EG, Beckmann KR, et al. Chromosomal localization of ARSB, the gene for human *N*-acetylga-lactosamine-4-sulphatase. Hum Genet. 1989; 82:67–68. [PubMed: 2714781]
2. Kunieda T, Simonaro CM, Yoshida M, et al. Mucopolysaccharidosis type VI in rats: isolation of cDNAs encoding arylsulfatase B, chromosomal localization of the gene, and identification of the mutation. Genomics. 1995; 29:582–587. [PubMed: 8575749]
3. Valayannopoulos V, Nicely H, Harmatz P, et al. Mucopolysaccharidosis VI. Orphanet J Rare Dis. 2010; 5:5. [PubMed: 20385007]
4. White KK. Orthopaedic aspects of mucopolysaccharidoses. Rheumatology (Oxford). 2011; 50:v26–v33. [PubMed: 22210667]
5. Simonaro, CM. Personal communications; 12th International Symposium on MPS and Related Diseases; The Netherlands: Noordwijkerhout; Jun 29. 2012
6. Smith LJ, Martin JT, Szczesny SE, et al. Altered lumbar spine structure, biochemistry, and biomechanical properties in a canine model of mucopolysaccharidosis type VII. J Orthop Res. 2010; 28:616–622. [PubMed: 19918911]
7. Jezyk PF, Haskins ME, Patterson DF, et al. Mucopolysaccharidosis in a cat with arylsulfatase B deficiency: a model of Maroteaux–Lamy syndrome. Science. 1977; 198:834–836. [PubMed: 144321]
8. Yoshida M, Ikadai H, Maekawa A, et al. Pathological characteristics of mucopolysaccharidosis VI in the rat. J Comp Pathol. 1993; 109:141–153. [PubMed: 8245230]
9. Yoshida M, Tachibana M, Kobayashi E, et al. The locus responsible for mucopolysaccharidosis VI (Maroteaux–Lamy syndrome) is located on rat chromosome 2. Genomics. 1994; 20:145–146. [PubMed: 8020950]
10. Haskins ME, Aguirre GD, Jezyk PF, et al. The pathology of the feline model of mucopolysaccharidosis VI. Am J Pathol. 1980; 101:657–674. [PubMed: 6778219]
11. Simonaro CM, D'Angelo M, Haskins ME, et al. Joint and bone disease in mucopolysaccharidoses VI and VII: identification of new therapeutic targets and biomarkers using animal models. Pediatr Res. 2005; 57:701–707. [PubMed: 15746260]

12. Simonaro CM, Haskins ME, Schuchman EH. Articular chondrocytes from animals with a dermatan sulfate storage disease undergo a high rate of apoptosis and release nitric oxide and inflammatory cytokines: a possible mechanism underlying degenerative joint disease in the mucopolysaccharidoses. Lab Invest. 2001; 81:1319–1328. [PubMed: 11555679]
13. Simonaro CM, Ge Y, Eliyahu E, et al. Involvement of the Toll-like receptor 4 pathway and use of TNF-alpha antagonists for treatment of the mucopolysaccharidoses. Proc Natl Acad Sci USA. 2010; 107:222–227. [PubMed: 20018674]
14. Yoshida M, Noguchi J, Ikadai H, et al. Arylsulfatase B-deficient mucopolysaccharidosis in rats. J Clin Invest. 1993; 91:1099–1104. [PubMed: 8450039]
15. Steenvoorden MM, Bank RA, Ronday HK, et al. Fibro-blast-like synoviocyte-chondrocyte interaction in cartilage degradation. Clin Exp Rheumatol. 2007; 25:239–245. [PubMed: 17543148]
16. Masuda K, Aota Y, Muehleman C, et al. A novel rabbit model of mild, reproducible disc degeneration by an anulus needle puncture: correlation between the degree of disc injury and radiological and histological appearances of disc degeneration. Spine. 2005; 30:5–14. [PubMed: 15626974]
17. Barbir A, Michalek AJ, Abbott RD, et al. Effects of enzymatic digestion on compressive properties of rat intervertebral discs. J Biomech. 2010; 43:1067–1073. [PubMed: 20116063]
18. Wilke HJ, Neef P, Caimi M, et al. New in vivo measurements of pressures in the intervertebral disc in daily life. Spine. 1999; 24:755–762. [PubMed: 10222525]
19. Espinoza Orias AA, Malhotra NR, Elliott DM. Rat disc torsional mechanics: effect of lumbar and caudal levels and axial compression load. Spine J. 2009; 9:204–209. [PubMed: 18495544]
20. Michalek AJ, Funabashi KL, Iatridis JC. Needle puncture injury of the rat intervertebral disc affects torsional and compressive biomechanics differently. Eur Spine J. 2010; 19:2110–2116. [PubMed: 20544231]
21. Sarver JJ, Elliott DM. Mechanical differences between lumbar and tail discs in the mouse. J Orthop Res. 2005; 23:150–155. [PubMed: 15607887]
22. Elliott DM, Sarver JJ. Young investigator award winner: validation of the mouse and rat disc as mechanical models of the human lumbar disc. Spine. 2004; 29:713–722. [PubMed: 15087791]
23. Smit TH, van Tunen MS, van der Veen AJ, et al. Quantifying intervertebral disc mechanics: a new definition of the neutral zone. BMC Musculoskelet Disord. 2011; 12:38. [PubMed: 21299900]
24. Beckstein JC, Sen S, Schaer TP, et al. Comparison of animal discs used in disc research to human lumbar disc: axial compression mechanics and glycosaminoglycan content. Spine (PhilaPa 1976). 2008; 33:E166–E173.
25. Grant JP, Oxland TR, Dvorak MF, et al. The effects of bone density and disc degeneration on the structural property distributions in the lower lumbar vertebral endplates. J Orthop Res. 2002; 20:1115–1120. [PubMed: 12382980]
26. Tommasini SM, Morgan TG, van der Meulen M, et al. Genetic variation in structure-function relationships for the inbred mouse lumbar vertebral body. J Bone Miner Res. 2005; 20:817–827. [PubMed: 15824855]
27. Panjabi MM. Clinical spinal instability and low back pain. J Electromyogr Kinesiol. 2003; 13:371–379. [PubMed: 12832167]
28. Crawley AC, Niedzielski KH, Isaac EL, et al. Enzyme replacement therapy from birth in a feline model of mucopolysaccharidosis type VI. J Clin Invest. 1997; 99:651–662. [PubMed: 9045867]
29. Adams MA, Roughley PJ. What is intervertebral disc degeneration, and what causes it? Spine. 2006; 31:2151–2161. [PubMed: 16915105]
30. Takahashi H, Suguro T, Okazima Y, et al. Inflammatory cytokines in the herniated disc of the lumbar spine. Spine (PhilaPa 1976). 1996; 21:218–224.
31. Lee S, Moon CS, Sul D, et al. Comparison of growth factor and cytokine expression in patients with degenerated disc disease and herniated nucleus pulposus. Clin Biochem. 2009; 42:1504–1511. [PubMed: 19563795]
32. Seguin CA, Pilliar RM, Roughley PJ, et al. Tumor necrosis factor-alpha modulates matrix production and catabolism in nucleus pulposus tissue. Spine (PhilaPa 1976). 2005; 30:1940–1948.

33. Schuerwegh AJ, Dombrecht EJ, Stevens WJ, et al. Influence of pro-inflammatory (IL-1 alpha, IL-6, TNF-alpha, IFN-gamma) and anti-inflammatory (IL-4) cytokines on chondrocyte function. Osteoarthritis Cartilage. 2003; 11:681–687. [PubMed: 12954239]
34. Purmessur D, Freemont AJ, Hoyland JA. Expression and regulation of neurotrophins in the nondegenerate and degenerate human intervertebral disc. Arthritis Res Ther. 2008; 10:R99. [PubMed: 18727839]
35. Abe Y, Akeda K, An HS, et al. Proinflammatory cytokines stimulate the expression of nerve growth factor by human intervertebral disc cells. Spine (PhilaPa 1976). 2007; 32:635–642.
36. Freemont AJ, Watkins A, Le Maitre C, et al. Nerve growth factor expression and innervation of the painful intervertebral disc. J Pathol. 2002; 197:286–292. [PubMed: 12115873]
37. Hayashi S, Taira A, Inoue G, et al. TNF-alpha in nucleus pulposus induces sensory nerve growth: a study of the mechanism of discogenic low back pain using TNF-alpha-deficient mice. Spine (PhilaPa 1976). 2008; 33:1542–1546.
38. Blanco FJ, Ochs RL, Schwarz H, et al. Chondrocyte apoptosis induced by nitric oxide. Am J Pathol. 1995; 146:75–85. [PubMed: 7856740]
39. Nakagawa S, Arai Y, Mazda O, et al. N-acetylcysteine prevents nitric oxide-induced chondrocyte apoptosis and cartilage degeneration in an experimental model of osteoarthritis. J Orthop Res. 2010; 28:156–163. [PubMed: 19725096]
40. Yurube T, Takada T, Suzuki T, et al. Rat tail static compression model mimics extracellular matrix metabolic imbalances of matrix metalloproteinases, aggrecanases, and tissue inhibitors of metalloproteinases in intervertebral disc degeneration. Arthritis Res Ther. 2012; 14:R51. [PubMed: 22394620]
41. Wang DL, Jiang SD, Dai LY. Biologic response of the intervertebral disc to static and dynamic compression in vitro. Spine. 2007; 32:2521–2528. [PubMed: 17978649]
42. Barak MM, Weiner S, Shahar R. The contribution of trabecular bone to the stiffness and strength of rat lumbar vertebrae. Spine (PhilaPa 1976). 2010; 35:E1153–E1159.
43. Tommasini SM, Hu B, Nadeau JH, et al. Phenotypic integration among trabecular and cortical bone traits establishes mechanical functionality of inbred mouse vertebrae. J Bone Miner Res. 2009; 24:606–620. [PubMed: 19063678]

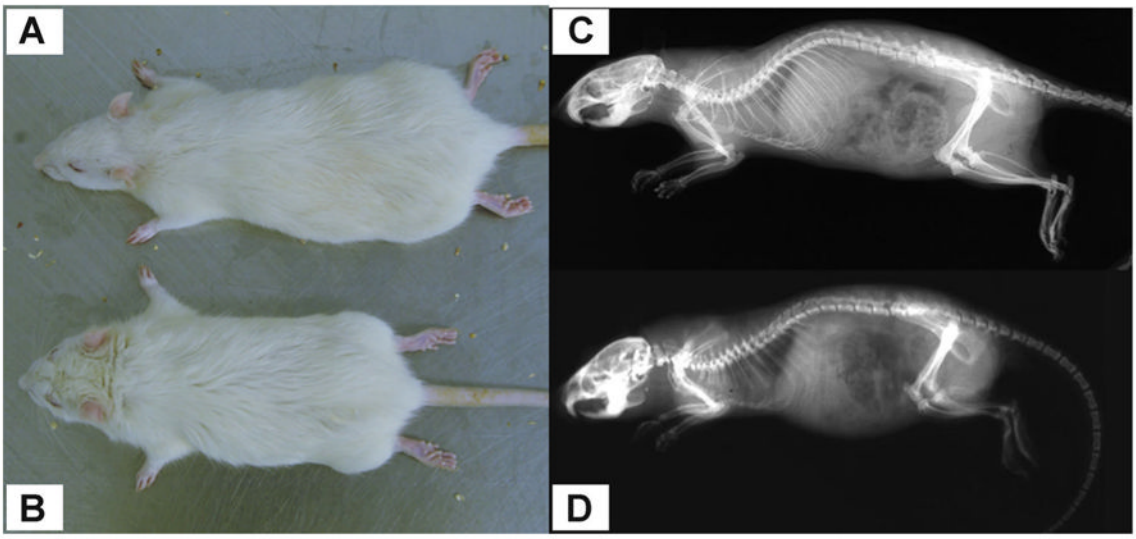

Figure 1.
(A) Normal and (B) MPS Sprague–Dawley rats (male, 6 months old). Radiographs of (C) normal and (D) MPS rat.

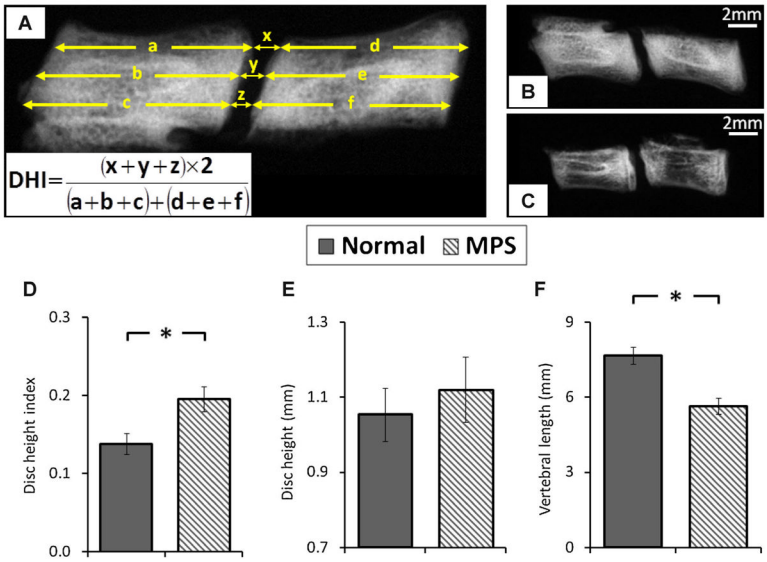

Figure 2.

(A) Measurement of disc height index (DHI) for L5–6 motion segment. Radiographs of (B) normal and (C) MPS motion segment. Comparison of (D) disc height index, (E) disc height, and (F) vertebral length between normal and MPS specimens. Error bar indicates standard deviation and * indicates significant difference ($p < 0.05$).

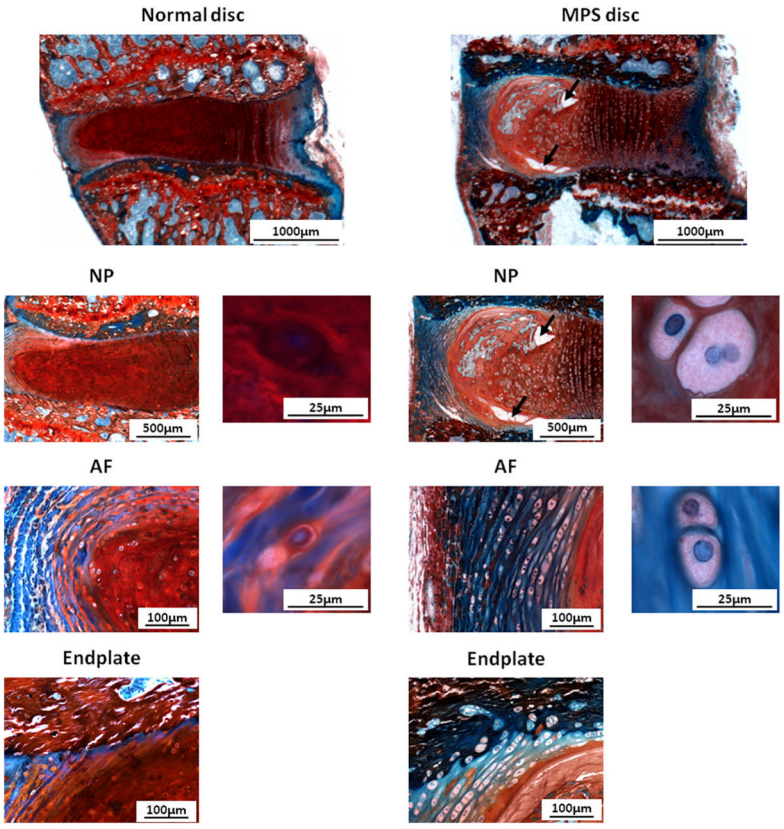

Figure 3.

Safranin-O/Fast-Green/hematoxylin staining for NP, AF, and endplate of normal and MPS discs. Compared to normal disc, MPS disc did not have signs of 'age-related degeneration', the annular lamellae were well organized and surrounded the NP with a clear nuclear/annular boundary. However, in MPS discs the NP contained sizable defects (black arrows), AF layers were thicker, and the endplate contained irregularities and less Safranin-O staining. The height of the MPS disc was also slightly larger. NP and AF cells of MPS VI rats were large and vacuolated, with less Safranin-O staining than for controls.

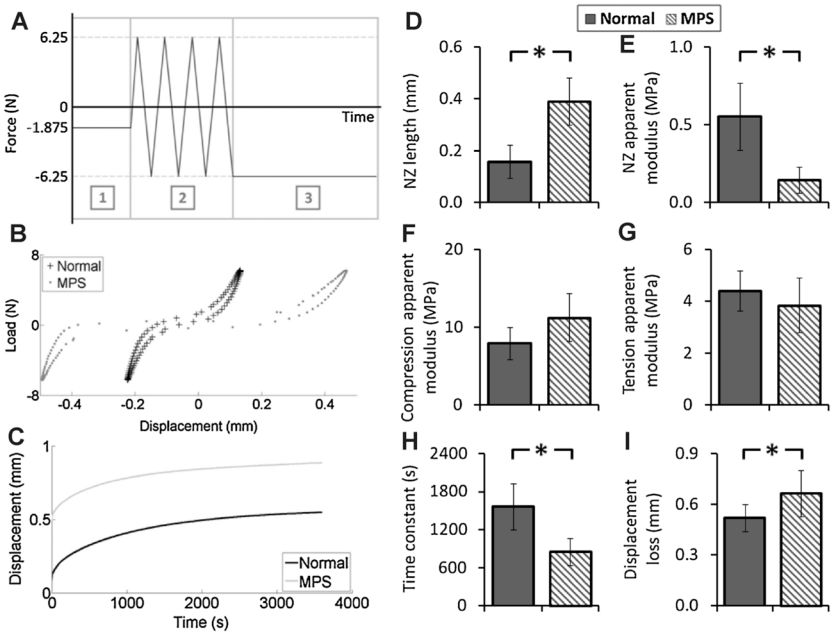

Figure 4.

(A) Loading protocol of axial testing: (1) equilibration with loading magnitude at −1.875 N for 30 min, (2) cyclic tension-compression test with loading magnitude of ±6.25 N at 1 Hz for 20 cycles, and (3) creep test with loading magnitude at −6.25 N for 60 min. (B) Representative load-displacement cycle obtained from cyclic test (20th cycle) of normal and MPS vertebra-disc-vertebra motion segments. (C) Representative creep behavior for normal and MPS vertebra-disc-vertebra motion segments. Results of cyclic test (D) neutral zone length, (E) neutral zone apparent modulus, (F) compression apparent modulus, and (G) tension apparent modulus. Results of (H) creep time constant, and (I) overall displacement loss throughout all test stages of the axial experiment. Error bar indicates standard deviation and * indicates significant difference ($p < 0.05$).

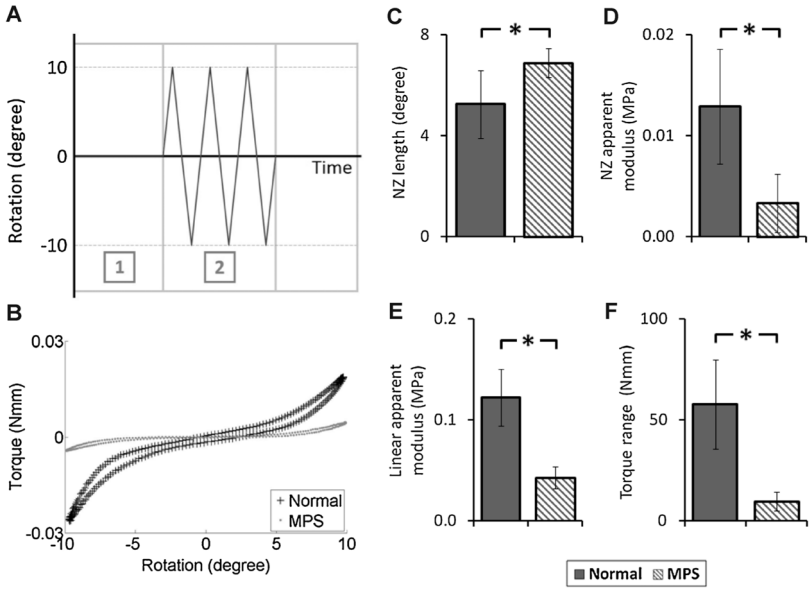

Figure 5.

(A) Loading protocol of torsional experiment: (1) equilibration with loading magnitude at −1.875 N for 30 min and (2) cyclic rotation test with rotational magnitude of ±10°at 1 Hz for 10 cycles. (B) Representative torque-rotation cycle obtained from cyclic rotation test (10th cycle) of normal and MPS vertebra-disc-vertebra motion segments. Results of cyclic rotation test (C) neutral zone length, (D) neutral zone apparent modulus, (E) linear apparent modulus, and (F) torque range. Error bar indicates standard deviation and * indicates significant difference ($p < 0.05$).

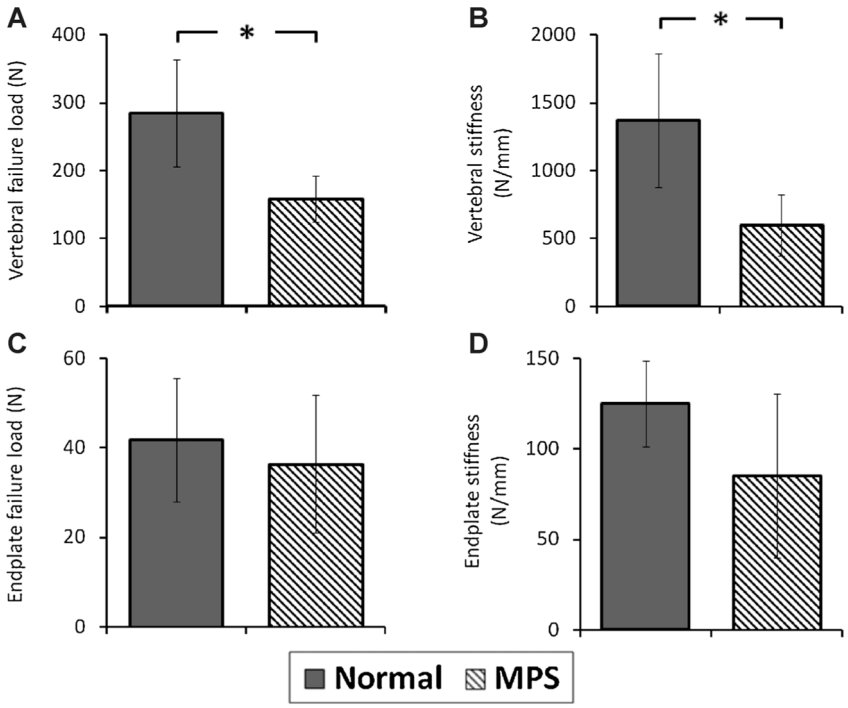

Figure 6.

Biomechanical properties of vertebral and vertebral endplate of normal and MPS specimens. (A) Vertebral failure load and (B) vertebral stiffness. (C) Endplate failure load and (D) endplate stiffness. Error bar indicates standard deviation and * indicates significant difference ($p < 0.05$).

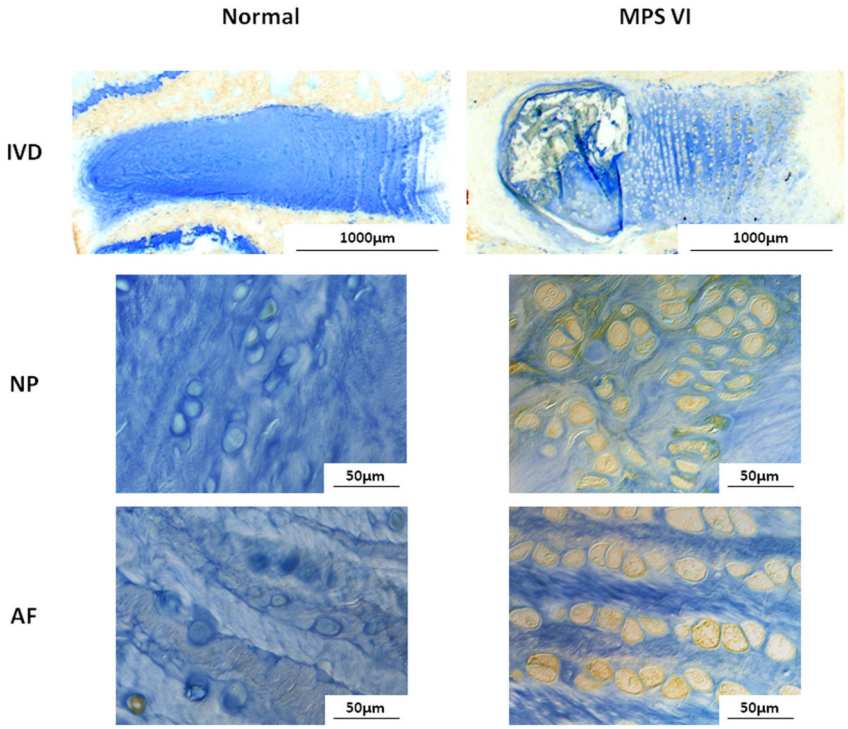

Figure 7.
Immunohistochemical staining for ADAMTS-5 for NP and AF of normal and MPS discs. Compared to normal disc, there were notably elevated ADAMTS-5-expressing cells in both NP and AF of MPS disc.

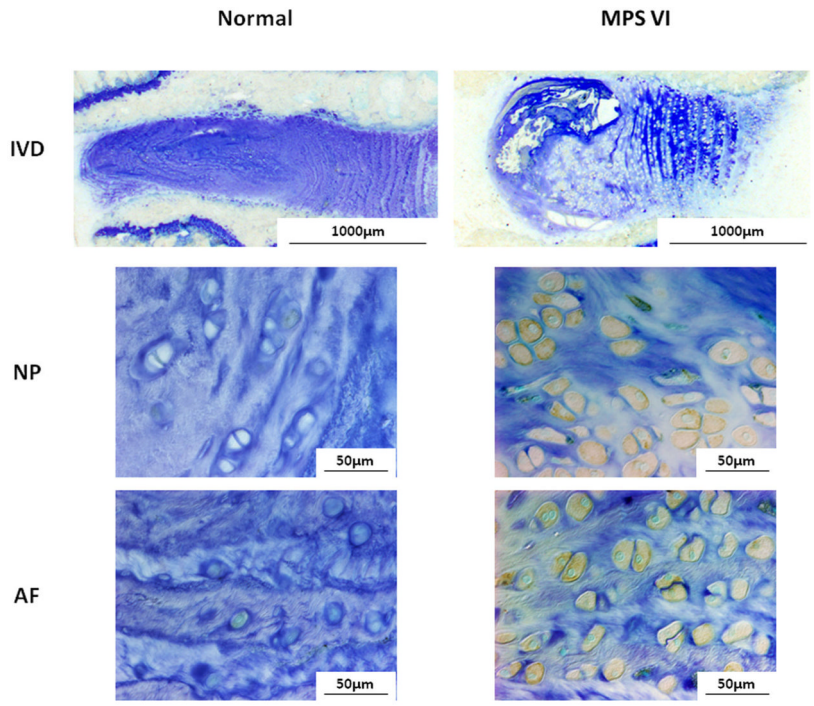

Figure 8.
Immunohistochemical staining for MMP-13 for NP and AF of normal and MPS discs. There were notably increased MMP-13 immunopositive cells in both NP and AF of MPS disc.

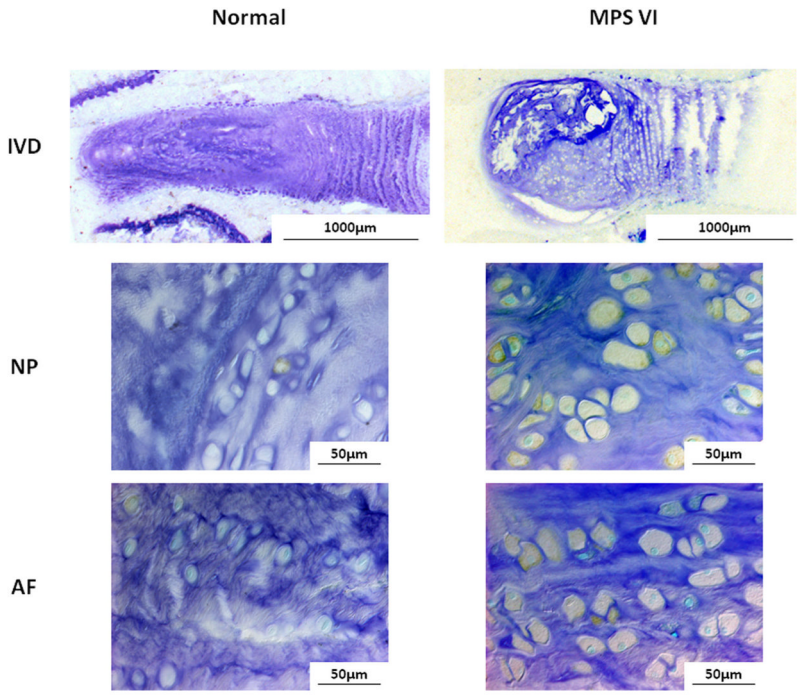

Figure 9.
Immunohistochemical staining for TNF-α for NP and AF of normal and MPS discs. MPS discs had greater immunostaining in both NP and AF cells when compared to normal discs.